Oxygen ion energy distribution: Role of ionization, resonant, and nonresonant charge-exchange collisions

N. Yu. Babaeva and J. K. Lee[a)]
Department of Electronic and Electrical Engineering, Pohang University of Science and Technology, Pohang 790-784, South Korea

J. W. Shon and E. A. Hudson
Lam Research Corporation, 4650 Cushing Parkway, Fremont, California 94538

(Received 21 October 2004; accepted 2 May 2005; published 21 June 2005)

Capacitively coupled rf discharge operating in oxygen/argon mixtures has been investigated using the particle-in-cell/Monte Carlo method. The roles of ionization, resonant and nonresonant charge-exchange collisions in the formation of ion energy distribution (IED) at the electrodes is investigated. By turning off/on the corresponding collisional processes, it is shown that ionization can play an essential role in formation of the IED structure. The relative contribution of ionization to IED is estimated. © *2005 American Vacuum Society.* [DOI: 10.1116/1.1943451]

I. INTRODUCTION

The extensive use of the capacitively coupled radio frequency discharges in the microelectronic industry for obtaining extraordinarily small feature sizes in the etching process has motivated extensive theoretical study and numerical modeling of these plasma sources.[1–5] Plasma chemical issues are important in the further optimization of the etching process. Feed gas mixtures are usually complex because of conflicting requirements on the etch rate, selectivity to photoresist (PR), and anisotropy. In the present paper, computational study of a capacitively coupled plasma source is presented operating in oxygen/argon mixtures. Oxygen discharges and their mixtures with argon and other gases are frequently used in the microelectronic industry to sputter deposit aluminum, tungsten, or high-temperature superconductivity films. Oxygen discharges can be used to grow SiO_2 films on silicon, or in etch and ash processes to remove PR and polymer films. Such electronegative discharges are under extensive study nowadays.[6,7]

In the present article two sets of simulation results are given. One is for high-oxygen/low-argon concentration mixture ($Ar:O_2=5\%:95\%$), the other one is for low-oxygen/high-argon concentration ($Ar:O_2=70\%:30\%$). We investigate the role of different processes important for ion energy distribution function (IEDF) on the electrodes. For this study, a one-dimensional electrostatic particle-in-cell Monte Carlo collisions (PIC/MCC) code XPDC1 has been used. The code was developed and validated by Plasma Theory and Simulation Group, University of California, Berkeley and modified by Plasma Application Modeling Group, Pohang University of Science and Technology to include the chemical coupling reactions between argon and oxygen. The PIC/MCC method[8] is a self-consistent kinetic method capable of the predicting electron energy distribution function and ion energy distribution function for ions arriving at the electrodes.

[a)]Electronic mail: jkl@postech.ac.kr

II. THE MODEL

We have simulated the operation of a capacitively coupled plasma source using a one-dimensional cylindrical model. The cylindrical electrodes model to the first approximation the asymmetric discharge with electrode area ratio 1.73. For this case the inner radius of the cylindrical electrode is $r_1=0.0274$ m, while the outer radius is $r_2=0.0474$ m. The Ar/O_2 discharge is maintained in a chamber between the two electrodes separated by a gap of 0.02 m. The schematic diagram of the reactor is presented in Fig 1. The inner (small) electrode is capacitively coupled to rf power supply through a blocking capacitor. The outer (large) electrode is grounded. Such a reactor is asymmetric in the sense that the grounded electrode is larger than the powered one. The wafer or substrate to be processed would be located on the inner (powered) electrode. We trace the plasma parameters along the r axis. Distribution of ion energy is considered at the inner and outer electrode surfaces. For the most results reported here the operating parameters are a pressure of 26 mTorr, applied voltage (amplitude) of 900 V, and rf frequency of 27 MHz. In the present study, the large electrode and the sheath at the large electrode are referred to as the RHS electrode and RHS sheath, correspondingly. The LHS electrode and LHS sheath correspond to the inner (small) electrode.

In an oxygen discharge, a number of species are formed. The species modeled in the present article are electrons, oxygen positive ions O_2^+, oxygen negative ions O^-, argon ions Ar^+, excited argon atoms Ar^*, excited oxygen molecules O_2^* (denoting various rotational, vibrational, and electronic states), and background argon atoms and oxygen molecules. The total reaction scheme includes 33 reactions among them. However, we trace concentrations of only four charged species (electrons, O_2^+, Ar^+, and O^- ions). Note that the main channel for negative ions formation is two-body dissociative attachment [reaction (15) in Table I]. The molecular negative ions O_2^- are primarily formed in three-body reactions. For low-pressure discharges the probability for these reactions to

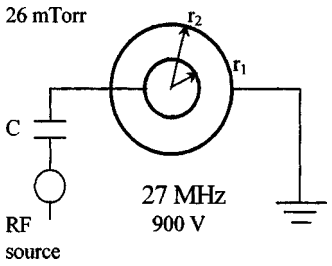

FIG. 1. Schematic diagram of cylindrical capacitively coupled plasma source.

occur is very small. Metastable Ar atoms are not considered here. At low pressure (<0.05 Torr) those metastables have little influence on the discharge parameters.

The chemical coupling reactions between argon and oxygen include charge exchange (CX) between neutral Ar and oxygen ion O_2^+, charge exchange between neutral oxygen O_2 and argon ion Ar^+, scattering of positive and negative oxygen ions on argon neutrals, scattering of Ar^+ ions on oxygen neutrals, and charge recombination.

TABLE I. Argon-oxygen reaction scheme used in PIC/MCC simulation.

N	Reaction	Energy loss (eV)	Description
(1)	$e+O_2=e+O_2^{*a}$	0.02	Rotational excitation
(2)	$e+O_2=e+O_2^*$	0.19	Vib. Excitation $\nu=1$
(3)	$e+O_2=e+O_2^*$	0.38	Vib. Excitation $\nu=2$
(4)	$e+O_2=e+O_2^*$	0.57	Vib. Excitation $\nu=3$
(5)	$e+O_2=e+O_2^*$	0.75	Vib. Excitation $\nu=4$
(6)	$e+O_2=e+O_2^*$	0.977	O_2 SING DELTA
(7)	$e+O_2=e+O_2^*$	1.627	O_2 B SING SIGMA
(8)	$e+O_2=e+O_2^*$	4.5	eExitation
(9)	$e+O_2=e+O_2^*$	6.0	eExitation
(10)	$e+O_2=e+O_2^*$	8.4	eExitation
(11)	$e+O_2=e+O_2^*$	9.97	eExitation
(12)	$e+O_2=2e+O_2^+$	12.06	Ionization
(13)	$e+O_2=e+O_2$	14.7	130 nm line exitation
(14)	$e+O_2=e+O_2$		MT[b]
(15)	$e+O_2\rightarrow O^-+O$		Diss. attachment
(16)	$O^-+O_2\rightarrow O_2+O+e$		Detachment
(17)	$O^-+O_2\rightarrow O^-+O_2$		MT
(18)	$O_2^++O_2\rightarrow O_2+O_2^+$		Resonant CX[c]
(19)	$O_2^++O_2\rightarrow O_2^++O_2$		MT
(20)	$O^-+O_2^+\rightarrow O+O_2$		Recombination
(21)	$e+O_2^+\rightarrow O+O$		Diss. recombination
(22)	$e+O^-\rightarrow O+2e$		El. impact detachment
(23)	$e+Ar\rightarrow e+Ar$		MT
(24)	$e+Ar\rightarrow e+Ar^*$	11.55	Excitation
(25)	$e+Ar\rightarrow 2e+Ar+$	15.76	Ionization
(26)	$Ar++Ar\rightarrow Ar++Ar$		MT
(27)	$Ar^++Ar\rightarrow Ar+Ar^+$		Resonant CX
(28)	$O^-+Ar\rightarrow O^-+Ar$		MT
(29)	$O_2^++Ar\rightarrow O_2^++Ar$		MT
(30)	$O_2^++Ar\rightarrow O_2+Ar^+$		Nonresonant CX
(31)	$Ar^++O_2\rightarrow Ar^++O_2$		MT
(32)	$Ar^++O_2\rightarrow Ar+O_2^+$		Nonresonant CX
(33)	$O^-+Ar^+\rightarrow O+Ar$		Recombination

[a]O_2^* denotes various excited rotational, vibrational, or electronic states of oxygen molecules.
[b]MT=momentum transfer
[c]CX=charge exchange

In Table I, 33 potentially significant collisional reactions used in the model are presented with corresponding energy losses. The identification of energy losses with specific processes (dissociation, attachment, etc.) is uncertain.[1] Our analysis is based on the knowledge of corresponding cross sections. Whereas the cross sections for noble gases have been measured reasonably well, this is not the case for collisions in molecular gases. Many of the cross sections are based on semiempirical or semiclassical methods. The cross sections for binary processes among oxygen and argon species have mostly not been measured carefully or calculated. Some data for electron impact excitation of O_2 (momentum transfer, rotational, vibrational excitation, two-body dissociative attachment, and excitation to states involving energy losses of 4.5, 6.0, 8.4, 9.97, and 14.7 eV, and ionization with an energy loss of 12.06 eV) were taken from Ref. 1. In this article, we concentrate only on reactions (12), (18), and (32).

We investigate four possible cases to study the role of these processes on IED formation at the electrode by successively turning them off and on. IED only for O_2^+ ions is considered.

We underline the importance of production of slow ions in the sheath region. There are typically three main processes that lead to generation of slow O_2^+ ions in the sheath, the first two of which are

$$O_2^+ + O_2 \Rightarrow O_2 + O_2^+ \ [\text{reaction(18)}],$$

$$Ar^+ + O_2 \Rightarrow Ar + O_2^+ \ [\text{reaction(32)}].$$

In the present article, it is shown that ionization in the sheath region,

$$e + O_2 \Rightarrow 2e + O_2^+ \ [\text{reaction(12)}],$$

also contributes to the formation of numerous IED peaks. We assume that ions created due to the ionization have Maxwellian distribution at a common temperature near room temperature (300 K). Note that additional process that can produce slow oxygen ions in the sheath region is UV ionization. This particular process is not considered here. The nonresonant CX process involving fast O_2^+ ions and slow Ar neutrals (reaction 30) does not contribute to IED of O_2^+ as the products of this reaction are slow Ar^+ ions but not O_2^+ ions.

The typical form of IED often exhibits numerous peaks that are primarily the result of CX collisions. A positive ion can collide with an atom, resulting in a transfer of the electron from the atom to the ion.[1] If the atom and ion are parent and child, the process of CX is resonant, as in reaction (18). Otherwise, the process is usually nonresonant; for example, reaction (32). In the CX process the collision between a fast ion and slow neutral yields a fast neutral and slow ion. Resonant CX (or symmetric CX) collisions will lead to a complete loss of the energy of the ion, which is taken over by the neutral of the same species. Thus, CX results in the formation of very slow ions and atoms having an energy practi-

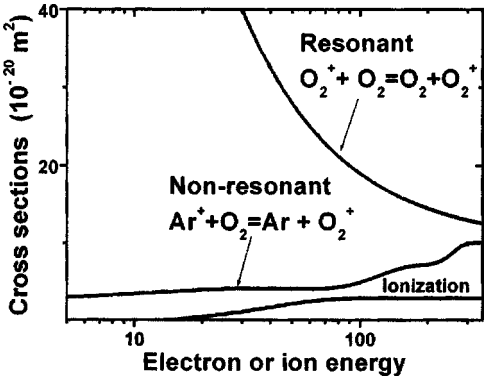

FIG. 2. Cross sections for processes (12), (18), and (32) as a function of collision energy.

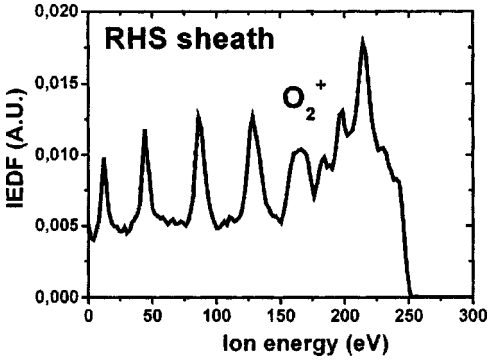

FIG. 3. IED at the large electrode (RHS). All the processes are taken into account, including resonant and nonresonant CX, and ionization.

cally equal to the initial energy of the ions. An ion becomes a neutral atom but retains its velocity. The atom, which has given up its electron to the ion and has become an ion, begins to drift in the field with zero initial velocity. This new ion travels until the next CX takes place. The process behaves as if a single ion were moving, which at each collision loses all of its drift kinetic energy.[9]

The mechanisms of CX reactions are rather well understood for resonant cases, where CX occurs at relatively large internuclear distances. In contrast, few nonresonant charge transfer reactions have been studied in detail and the mechanisms of this reaction type are still far from being understood completely. Because such reactions must involve electronic to translational, vibrational, or rotational energy coupling, they are intrinsically more difficult to characterize and understand.[10,11] Figure 2 demonstrates cross sections for reactions (12), (18), and (32) (see Refs. 10,11) used in the present study in the 10–300 eV collision energy range. The cross section for the nonresonant $Ar^+ + O_2$ reaction is shown to be much lower than for the resonant (symmetric) CX reaction.

III. RESULTS AND DISCUSSION

A. All the processes are included

When all the processes are included, the IED shows a typical collision-dominated profile with numerous peaks in the tail region (Fig. 3). The IEDF is normalized on the total number of ions arriving on the unit square of the electrode. The vertical axis indicates the normalized ion flux. As ions respond to a partially averaged potential, the IED spread corresponds roughly to the mean potential drop at the electrode. Elastic collisions result in the tail of lower energy ions, while CX collisions are the main contributor to the formation of a number of peaks.[12,13] The mechanism that generates the peaks is the oscillating front of the electron density. If a slow ion is created at a certain position, the electron density front may be between the ion position and the electrode. The ion is then in the quasineutral part with no electric field. When the electron front moves back (away from the electrode), the ion is accelerated towards the electrode. Thus, the ions are bunched and each successive rf cycle creates a new bunch. Note that slow oxygen ions can appear as products of reactions (12), (18), and (32).

B. Resonant CX collisions are turned off

When the resonant CX collision process 32 is turned off, the IED becomes almost collisionless, as shown in Fig. 4. The high-energy portion of O_2^+ ions dominates. However, the small peaks still exists. Are they due to the nonresonant CX collisions?

C. Resonant and nonresonant CX collisions are turned off

When processes (18) and (32) are turned off, the IED in Fig. 5 exhibits almost the same structure with small peaks as in Fig. 4. Reaction $Ar^+ + O_2 = Ar + O_2^+$ removes fast Ar^+ ions to produce slow O_2^+ ions. In this case the identity of the ion considered changes. However, the effect of the nonresonant CX collision is negligible in this case for two reasons. First of all, the nonresonant CX cross section is small.[10,11] In addition, in the mixture of 5% Ar and 95% O_2 there are not many argon neutrals to collide with oxygen ions O_2^+. Below, we show that the effect is small even for the more argon-abundant mixture (70% Ar). Thus, the existence of small peaks has to be explained by another mechanism producing slow ions in the sheath. Are the peaks due to ionization?

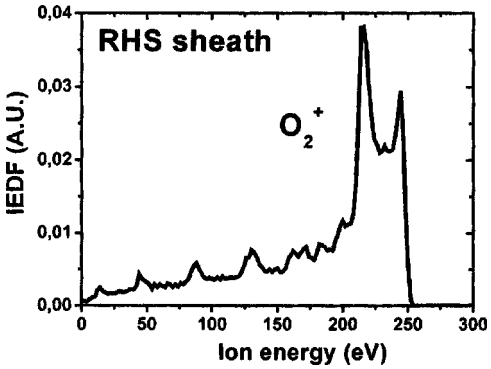

FIG. 4. IED at the large electrode (RHS). The resonant CX collision process (18) is turned off. Much smaller peaks still exist.

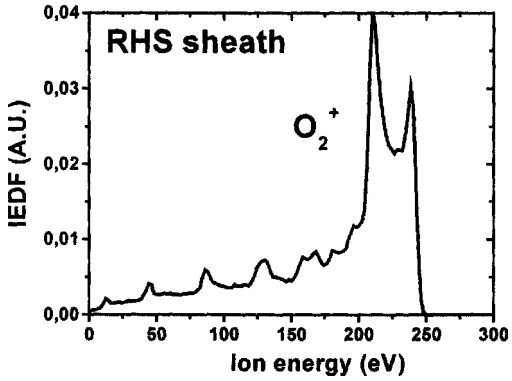

FIG. 5. IED at the upper electrode (RHS). Resonant CX [reaction (18)] and nonresonant [reaction (32)] collisions are turned off. Almost the same structure as in Fig. 4 with small peaks in the tail region.

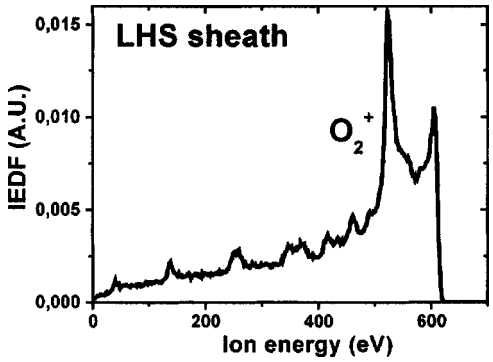

FIG. 7. IED at the LHS electrode for the same conditions as in Fig 6. The peaks still exist.

D. Ionization is turned off in the RHS sheath

For the final case, reactions (18) and (32) are turned off and, additionally, O_2 ionization [reaction (12)] is turned off in the RHS sheath. Note that O_2 ionization cannot be turned off in the whole discharge region as no discharge will be sustained in this case. Figure 6 demonstrates the disappearance of most peaks in the IEDF for the RHS sheath if there is no ionization in the sheath region. A simple bimodal ion energy distribution is observed. This typical bimodal structure is due to the rf modulation of the ion energy as the ions traverse the sheath. However, the lower-energy peaks persist in the IEDF for the LHS sheath where there is still ionization, as shown in Fig. 7. The Monte Carlo ionization profile for this particular case is plotted in Fig. 8 and shows the number of ionization events per unit volume per unit time. Thus, the conclusion can be made that ionization in the sheath region also contributes to the fine structure of ion energy distribution. In the process of ionization, certain amount of slow ions having thermal velocities are produced. In this sense, the ionization process is analogous to CX collisions when slow oxygen ions are generated in the sheath. The relative contribution to the production of slow ions is different for reactions (12), (18), and (32).

The same procedure of turning off the reactions (12), (18), and (32) is repeated for a greater Ar mixing ratio. Figures 9(a), 9(b), 9(c), and 9(d) present the results for 70% Ar:30% O_2 mixture and reveal the same dependence of the IEDF shape on collisional processes. However, in this case the influence of nonresonant CX collisions is greater due to a greater concentration of Ar species.

E. How plasma parameters change

Note that when turning off the processes (12), (18), and (32), we inevitably change the discharge parameters: the sheath structure, sheath thickness, plasma potential, plasma composition, etc. However, these changes are rather small and are not critical for our consideration. Figure 10 shows the comparison of plasma composition for 5% Ar:95% O_2 when all the process are taken into account and some of the collision processes are absent. The structure of the discharge is typically electronegative and is characterized by the presence of negative ions O^- . The dominant charged species are O_2^+ and O^-. The negative ions are trapped in the plasma bulk. The electron density in the discharge is much smaller due to attachment processes. In the absence of all the three processes [Fig. 10(b)], electron and ion concentration are slightly depleted in the RHS sheath. The plasma bulk becomes wider. Despite no ionization events in the sheath, electrons and ions (which are created in the bulk or even in the left sheath) arrive at the right sheath region due to their mobility. In addition, there is a small amount of electrons created due to the ionization of Ar atoms as this process is

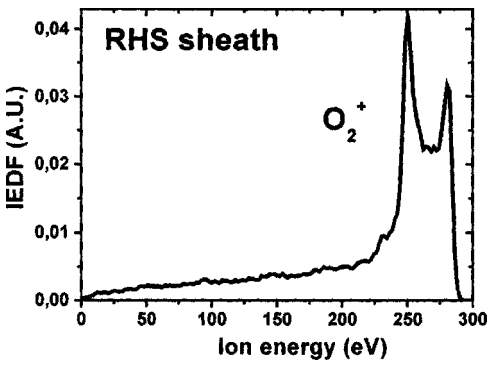

FIG. 6. IED at the RHS electrode. Processes (18) and (32) are turned off. In addition, ionization is turned off in the RHS sheath. The peaks disappeared.

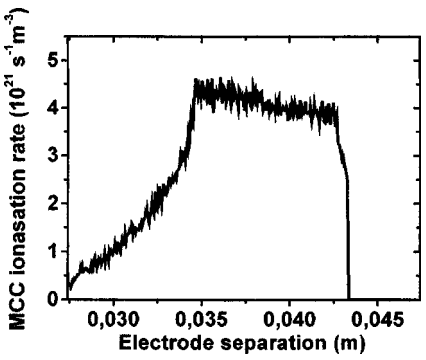

FIG. 8. Ionization rate with the absence of ionization events in the RHS sheath (no ionization events at $r > 0.0433$ m).

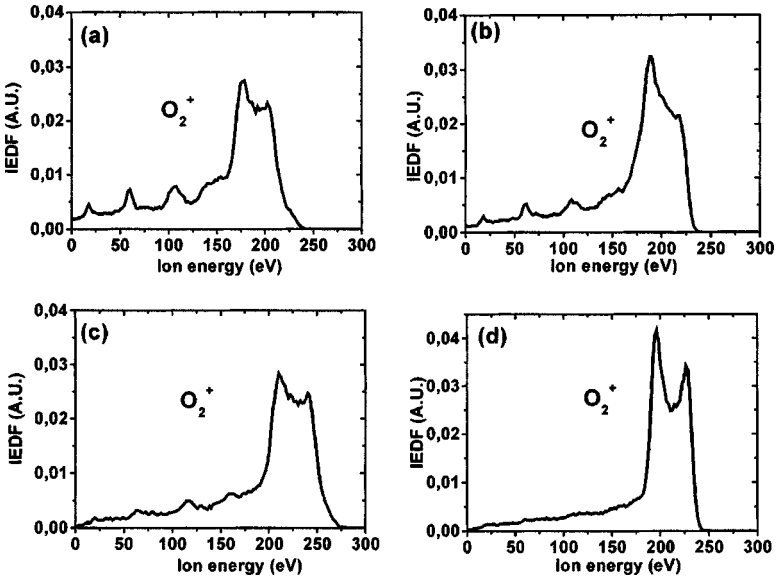

FIG. 9. Effect of collisions on IED for 70% Ar:30% O_2 mixture. (a) All the processes are included. (b) No resonant CX collisions. (c) No resonant and no nonresonant CX collisions. The influence of nonresonant CX collisions is slightly greater compared to low argon case. (d) No resonant and no nonresonant CX collisions. In addition, ionization is turned off in the RHS sheath. The peaks disappeared.

not turned off. The relative abundance of the ions (O_2^+, O^-, Ar^+) and electrons maintains the relation $\%O_2^+ > \% O^- > \text{electrons} > Ar^+$.

For argon-rich discharges (70 % Ar:30% O_2), the sheath width decreases and the plasma bulk becomes wider in comparison with 5% Ar:95% O_2 (Fig. 11). Negative ions are still the main dominant ions in this case with slightly less Ar^+ ion concentration. The absence of the reactions (18), (32), and (12) in the RHS sheath changes the plasma composition, as shown in Fig. 11(b). In this case, the relative abundance of ions (O_2^+, O^-, Ar^+) and electrons maintains the relation $\% O^- > \% Ar^+ > O_2^+ > \text{electrons}$. Potential profiles for 5% Ar:95% O_2 mixtures typical for asymmetric discharge are shown in Fig. 12. The potential drop at the smaller electrode (LHS sheath) is larger than that at the large electrode (RHS sheath). The dashed line shows how the potential is slightly changed when processes (12), (18), and (32) are not included.

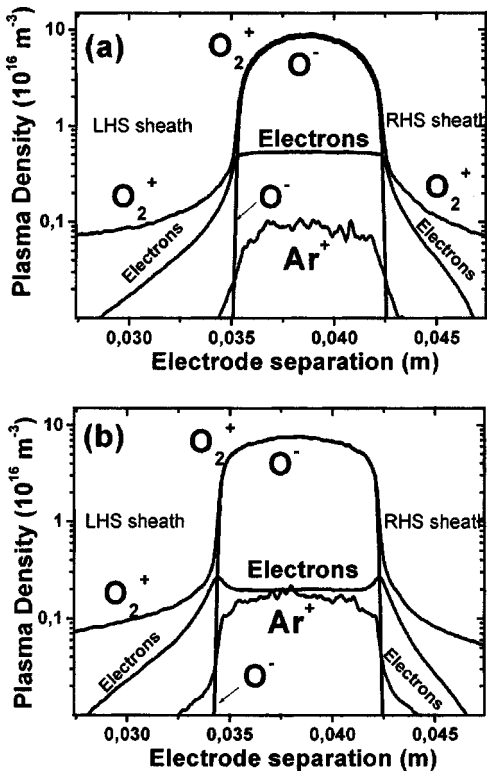

FIG. 10. Plasma composition profiles for 5% Ar:95% O_2 mixture. (a) All the process are taken into account. (b) No resonant CX and nonresonant CX collisions. Ionization is also turned off in the RHS sheath.

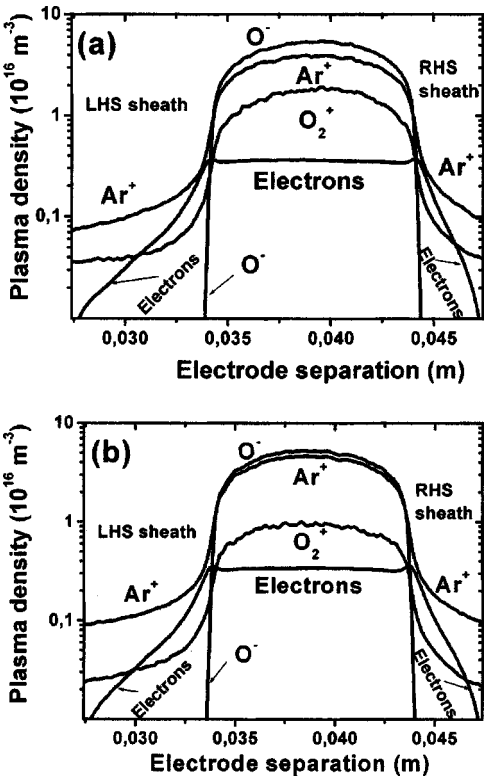

FIG. 11. Plasma composition profiles for 70% Ar:30% O_2 mixture. (a) All the process are included. (b) No resonant CX and nonresonant CX collisions. Ionization is also turned off in the RHS sheath.

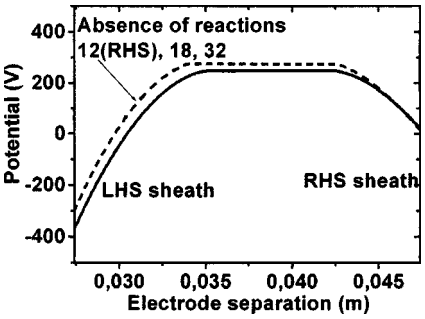

FIG. 12. Potential profiles for 5% Ar:95% O_2 mixtures typical for asymmetric discharge. Potential drop at the smaller electrode (LHS sheath) is larger than that at the large electrode (RHS sheath). Dashed line shows how the potential is changed when processes (12), (18), and (32) are not included.

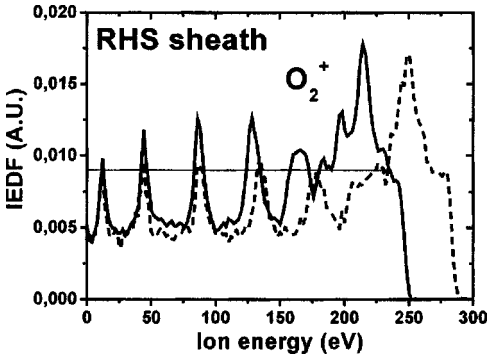

FIG. 13. IED at the RHS electrode for 5% Ar:95% O_2 mixture. All the processes are included (solid line), only ionization in the RHS sheath is turned off (dashed line), but the processes (18) and (32) are still included. The peaks above the horizontal straight line show the relative contribution of ionization process to IED.

F. Contribution of ionization to IEDF

To estimate the contribution of the ionization process to the IED formation, a comparison is made of two cases when (i) all the processes are included and (ii) only ionization in the RHS sheath is turned off. The results are presented in Fig. 13. The curves are shifted relative to each other due to inevitable small changes in the sheath size. The peaks above the horizontal straight line show the relative contribution of the ionization process to IED. The effect of ionization is small but not negligible.

IV. CONCLUSIONS

In conclusion, the role of ionization, resonant and nonresonant charge-exchange collisions in the formation of ion energy distribution at the electrodes is investigated. It is shown that ionization can play an essential role in the formation of the IED structure. The relative contribution of ionization into IEDF is estimated. To the authors' knowledge, it is impossible to conduct an experiment in which the processes such as ionization can be turned off in one of the sheath regions. In this connection, simulations give significant insight to our understanding of the main processes responsible for IEDF formation.

ACKNOWLEDGMENTS

The authors thank Dr. Zoran Raspopovic for implementing argon-oxygen Monte Carlo collisions in the oxygen *XPDC1* code. This work was supported in part by the Lam Research Corporation, Samsung Electronics, and Teralevel Nano Devices Project, 21c Frontier R&D Program of Korea Ministry of Science and Technology.

[1]M. A. Lieberman and A. J. Lichtenberg, *Principles of Plasma Discharges and Material Processing* (Wiley, New York, 1994).
[2]H. C. Kim and J. K. Lee, Phys. Rev. Lett. **93**, 085003 (2004).
[3]H. C. Kim, J. K. Lee, and J. W. Shon, Appl. Phys. Lett. **84**, 864 (2004).
[4]T. Makabe and Z. Lj. Petrovic, in *Advances in Low Temperature RF Plasmas*, edited by T. Makabe (Elsevier, New York, 2002), pp. 88–114.
[5]J. K. Lee, N. Yu. Babaeva, H. C. Kim, O. V. Manuilenko, and J. W. Shon, IEEE Trans. Plasma Sci. **32**, 47 (2004).
[6]C Lee and M. A. Lieberman, J. Vac. Sci. Technol. A **13**, 368 (1995).
[7]C Lee, M. A. Lieberman, A. J. Lichtenberg, F. Bose, H. Baltes, and R. Patrick J. Vac. Sci. Technol. A **15**, 113 (1997).
[8]C. K. Birdsall and A. B. Langdon, *Plasma Physics via Computer Simulation* (Adam Hilger, New York, 1991).
[9]S. C. Brown, *Basic Data of Plasma Physics. The Fundamental Data on Electrical Discharges in Gases* (AIP, New York, 1994).
[10]O. Dutuit, C. Alcaraz, D. Gerlich, P. M. Guyon, J. Hepburn, C. Metayer-Zeitoun, J. B. Ozenne, M. Schweizer, and T. Weng, Chem. Phys. **209**, 177 (1996).
[11]G. D. Flesch, S. Nourbakhsh, and C. Y. Ng, J. Chem. Phys. **92**, 3590 (1990).
[12]C. Wild and P. Koidl, Appl. Phys. Lett. **54**, 505 1989.
[13]W. J. Goedheer, Plasma Sources Sci. Technol. **9**, 507 (2000).